



HAL
open science

Overall Structures of Mycobacterium tuberculosis DNA Gyrase Reveal the Role of a Corynebacteriales GyrB-Specific Insert in ATPase Activity

Stéphanie Petrella, Estelle Capton, Bertrand Raynal, Clément Giffard, Aurélien Thureau, Françoise Bonneté, Pedro Alzari, Alexandra Aubry, Claudine Mayer

► To cite this version:

Stéphanie Petrella, Estelle Capton, Bertrand Raynal, Clément Giffard, Aurélien Thureau, et al.. Overall Structures of Mycobacterium tuberculosis DNA Gyrase Reveal the Role of a Corynebacteriales GyrB-Specific Insert in ATPase Activity. *Structure*, 2019, 27 (4), pp.579-589.e5. 10.1016/j.str.2019.01.004 . hal-02360258

HAL Id: hal-02360258

<https://hal.science/hal-02360258>

Submitted on 22 Oct 2021

HAL is a multi-disciplinary open access archive for the deposit and dissemination of scientific research documents, whether they are published or not. The documents may come from teaching and research institutions in France or abroad, or from public or private research centers.

L'archive ouverte pluridisciplinaire **HAL**, est destinée au dépôt et à la diffusion de documents scientifiques de niveau recherche, publiés ou non, émanant des établissements d'enseignement et de recherche français ou étrangers, des laboratoires publics ou privés.



Distributed under a Creative Commons Attribution - NonCommercial 4.0 International License

Overall structures of *Mycobacterium tuberculosis* DNA gyrase reveal the role of a *Corynebacteriales* GyrB specific insert in ATPase activity

AUTHORS

Stéphanie Petrella^{1,2,3,a,*}, Estelle Capton⁴, Bertrand Raynal^{2,5}, Clément Giffard^{1,2,3}, Aurélien Thureau⁶, Françoise Bonneté⁷, Pedro M. Alzari^{1,2,3}, Alexandra Aubry^{4,b,*}, Claudine Mayer^{1,2,3,b}

¹Institut Pasteur, Unité de Microbiologie Structurale, 25 rue du Docteur Roux, 75724 Paris Cedex 15, France

²CNRS UMR 3528, Biologie structurale des processus cellulaires et maladies infectieuses, Institut Pasteur, 75724 Paris Cedex 15, France

³Université Paris Diderot, Sorbonne Paris Cité, 75724 Paris Cedex 15, France

⁴Sorbonne Université, Centre d'immunologie et des maladies infectieuses-Paris, Cimi-Paris, INSERM U1135, National Reference Center for Mycobacteria, Laboratoire de Bactériologie-Hygiène, AP-HP, Hôpitaux Universitaires Pitié-Salpêtrière – Charles Foix, F-75013 Paris, France

⁵Institut Pasteur, Plateforme de biophysique moléculaire, Centre d'innovation et de recherche technologique, 25 rue du Docteur Roux, 75724 Paris Cedex 15, France ;

⁶Synchrotron SOLEIL, l'Orme des Merisiers, F-91410 Saint Aubin, France

⁷Institut de Biologie Physico-Chimique (IBPC) – LBPCPM UMR7099, 13 rue Pierre et Marie Curie, 75005 Paris, France

^a Lead Contact

* Correspondence: stephanie.petrella@pasteur.fr and alexandra.aubry@sorbonne-universite.fr

^b contributed equally to the work

SUMMARY

Despite sharing common features, previous studies have shown that gyrases from different species have been modified throughout evolution to modulate their properties. Here, we report two crystal structures of *Mycobacterium tuberculosis* DNA gyrase, an apo and AMPPNP-bound forms at 2.6-Å and 3.3-Å resolution, respectively. These structures provide high-resolution structural data on the quaternary organization and inter-domain connections of a gyrase (full-length GyrB-GyrA57)₂ thus providing crucial inputs on this essential drug target. Together with SAXS studies, they revealed an “extremely open” N-gate state, which persists even in the DNA-free gyrase-AMPPNP complex and an unexpected connection between the ATPase and cleavage-core domains mediated by two *Corynebacteriales*-specific motifs, respectively the C- and DEEE-loops. We show that the C-loop participates to the stabilization of this open conformation explaining why this gyrase has a lower ATPase activity. Our results image a conformational state which might be targeted for drug discovery.

KEYWORDS

Type IIA topoisomerases, *Mycobacterium tuberculosis*, DNA gyrase, *Corynebacteriales*, X-ray structure, ATPase activity, molecular machine, DNA binding protein, Fluoroquinolone

INTRODUCTION

Type II DNA topoisomerases are ubiquitous enzymes that manage DNA reorganization, and are therefore essential for many cellular events that take place during cell life (Schoeffler and Berger, 2008). Using ATP as a cofactor, they control DNA topology by adding or removing DNA supercoils and by tangling or knotting DNA. Topoisomerases achieve these topological rearrangements through a succession of dissociation/association events of three domain-dimerization interfaces, which function as open/closed 'gates', to allow the movement of one DNA duplex through another (Lanz and Klostermeier, 2011). The type IIA enzymes are found predominantly in bacteria and eukaryotes and share structural and evolutionary features (Corbett and Berger, 2004). DNA gyrase and topoisomerase (topo) IV are the type IIA enzymes expressed in bacteria (Schoeffler and Berger, 2008). Gyrase facilitates DNA unwinding at replication forks by introducing negative supercoils and topo IV has a specialized function in mediating the decatenation of interlocked daughter chromosomes (Levine et al., 1998). They are made up of two subunits, GyrA or ParC and GyrB or ParE, respectively, forming the catalytically active heterotetrameric enzymes (A_2B_2 or C_2E_2). GyrB and ParE subunits consist of two domains, the N-terminal ATPase and the C-terminal Toprim domains, whereas GyrA and ParC consist of the N-terminal breakage-reunion domain (BRD) followed by a C-terminal domain (CTD) (Figure 1A). Extensive studies have led to a general model for the catalytic cycle (Lindsley and Wang, 1993, Vos et al., 2011, Berger et al., 1996, Nitiss, 2009). However, many details remain unclear including both the conformation of the type IIA topoisomerase holoenzyme, in particular the structures of the various open and closed conformations, and the coordination of the enzyme catalytic cycle by ATP. Very low resolution structural data are available from electron

microscopy and small angle X-ray scattering (SAXS) (Baker et al., 2010, Costenaro et al., 2005, Kirchhausen et al., 1985, Papillon et al., 2013), but the only available X-ray crystal structures of full type II topoisomerases are those of the full-length topo II from yeast and topo IV from *Streptococcus pneumoniae*, solved at 4.4-Å and 3.7-Å resolution, respectively (Schmidt et al., 2012, Laponogov et al., 2013). The eukaryotic enzyme structure is in a closed conformation (with the three gates closed) whereas the topo IV structure displays an open clamp conformation (N-gate open) (Figure 2A). So far, high-resolution structures of a full-length DNA gyrase are still lacking.

Interestingly, *Mycobacterium tuberculosis* (*Mtb*), the causative agent of tuberculosis, encodes only one type II topoisomerase, i.e. DNA gyrase (Cole et al., 1998). As a result, the *Mtb* enzyme exhibits a different activity spectrum compared to other DNA gyrases, e.g. it supercoils DNA with efficiency comparable to that of other DNA gyrases, but shows enhanced relaxation, DNA-cleavage and decatenation activities (Aubry et al., 2006), and is the unique target of fluoroquinolones (FQ), the second line antibiotics used in the treatment of multi-drug resistant tuberculosis. To understand *Mtb* DNA gyrase specific activities and FQ resistance mechanisms, we and others have characterized the structures of the different individual domains (Piton et al., 2009, Piton et al., 2010, Darmon et al., 2012, Bouige et al., 2013, Roué et al., 2013, Agrawal et al., 2013, Tretter et al., 2010, Blower et al., 2016, Fu et al., 2009). These studies revealed several particular features of *Mtb* gyrases such as the presence of two unique motifs, DEEE- and DPP-loops in the BRD (Piton et al., 2010), the absence of a C-terminal control element found in *E. coli* gyrase (Tretter and Berger, 2012), the existence of a second GyrA-box motif implicated in the decatenation activity (Bouige et al., 2013), or yet, an insertion of a 32-residues

segment in the ATPase domain (Agrawal et al., 2013). This insert, hereafter termed C-loop, is found only in GyrB ATPase domains of *Corynebacteriales*. Largely disordered in the structure of isolated *Mtb* GyrB47 (Agrawal et al., 2013), this insert was suggested to mediate protein-protein interactions.

To define the global architecture of *Mtb* DNA gyrase, and to study the role of this insert in the context of the full-length B subunit in complex with the N-terminal domain of the A subunit (GyrB-GyrA57)₂, we determined the crystal structures of *Mtb* gyrase in its apo form at 2.6-Å resolution and in complex with a non-hydrolyzable ATP analog at 3.3-Å resolution. Comparison with the previously determined topo IV open clamp conformation revealed that both the apo and AMPPNP-bound structures adopt an almost identical “extremely open” conformation in which the ATPase domain is bent back and rotated to make several contacts with the Toprim and A-subunit regions. The unexpected absence of GyrB N-terminal dimerization in the presence of AMPPNP is further confirmed by structural studies in solution by SAXS. Besides, our crystal structures show that the C-loop is largely involved in the interactions between the ATPase domains and the DNA-binding-and-cleavage core thus stabilizing this specific *Mtb* DNA gyrase conformation probably corresponding to a resting state, in agreement with biochemical studies highlighting the lower basal ATP turnover of the enzyme.

RESULTS

“Extremely open” N-gate structure of *Mtb* DNA gyrase

The difficulty of characterizing the ATPase and DNA-binding-and-cleavage elements of type IIA topoisomerases derives from the large size and dynamic nature of these enzymes. In particular, each of the three dimerization interfaces can exist in an associated or dissociated state, resulting in a significant conformational variability in solution. To prevent subunit dissociation and to generate a more stable heterotetramer, we linked GyrB and GyrA57 into a single polypeptide chain (termed GyrBA57) leading to an enzyme (full-length GyrB-GyrA57)₂ with a total molecular weight of almost 260 kDa (Figure 1A). After extensive crystallization attempts using a combination of different ligands, including nonhydrolyzable ATP analog, fluoroquinolone and two different dsDNA substrates of varying length (see further details in the Methods section), we were able to obtain the crystal structures of an ‘apo’ and ‘holo’ (containing AMPPNP and Mg²⁺) forms of GyrBA57 (Table 1). The final models contain a full GyrBA57 dimer in the asymmetric unit (Figure 1B,C and Table 1). These two structures are almost identical with a global r.m.s.d. value of 1.2 Å (1719 C_α atoms), and overall dimensions of ~ 100 Å X 110 Å X 150 Å. Notably, the dimeric conformations of the DNA-binding-and-cleavage core in the two structures match those seen for the BRD and Toprim domain observed in isolation but also in complexes (Piton et al., 2010, Blower et al., 2016, Fu et al., 2009) (Figure S1A,B). However, an open N-gate conformation in a DNA-free state is observed for the GyrBA57 crystal structures (Figure 2). Whereas the open clamp conformation was expected because of the absence of DNA, the unexpected result is that this open conformation is maintained even in the presence of AMPPNP (Figure 1C).

The oligomerization state of GyrBA57 protein in solution, in absence or presence of AMPPNP, or without the C-loop (i.e. GyrBA57 $_{\Delta C\text{-loop}}$), was assessed by analytical ultracentrifugation. At all measured concentrations, the main peak had a sedimentation of 8.8, 9.6, 9.0 S and a frictional ratio (f/f_0) of 1.6, 1.4, 1.5 for the apo, AMPPNP-bound and $\Delta C\text{-loop}$ forms, respectively (Table S1). These data are compatible with a dimeric form for GyrBA57 irrespectively of the absence or presence of AMPPNP or the C-loop (Figure S2A). These experimental values are well below the calculated sedimentation of 10.4 and 10.5 S determined with GyrBA57 crystal structures of apo and AMPPNP-bound forms, respectively, indicating that the shapes of the proteins in solution and in crystals are not similar (Table S2). Furthermore, the theoretical sedimentation values calculated for a closed **N**-gate conformation based on yeast topo II (named GyrBA57 $_{\text{Nc}}$, Figure S3C) and an open **N**-gate conformation based on pneumococcal topo IV (named GyrBA57 $_{\text{No}}$) of 10.1 and 9.8 S (Table S2), are well above the experimental value of 8.8 S of the apo form, indicating that the apo GyrBA57 conformation in solution clearly differs from the closed or open N-gate conformations observed in other topoisomerase crystal structures. However, the theoretical sedimentation value of the GyrBA57 $_{\text{No}}$ is compatible with the experimental value of 9.6 S determined for nucleotide-bound GyrBA57 (9.8 S - Table S2), suggesting a similar conformation.

Further characterization of the protein structures in solution were performed using SAXS measurements (Figure 3A), in presence of both nucleotide and DNA (Konarev et al., 2003). However, we were unable to obtain interpretable scattering data of the protein in presence of DNA due to protein aggregation and conformational heterogeneity, possibly explaining why no crystals were obtained for the ternary complex. All SAXS experimental and analytical details are given in the

supplementary section (Table S1). Overall, a radius of gyration (R_g) of 58, 53, 55 Å with a maximal dimension (D_{max}) of 197, 183, 204 Å, were derived from the $P(r)$ distribution for apo, AMPPNP-bound, GyrBA57 $_{\Delta C-loop}$ enzymes, respectively (Figure 3B, Figure S2B and Table S3). The calculated molecular masses confirm that the two GyrBA57 and GyrBA57 $_{\Delta C-loop}$ enzymes are dimeric in solution (Table S1). Differences between the scattering curves collected for the apo and AMPPNP-bound states showed that nucleotide binding substantially alters holoenzyme conformation (Figure 3A). The $P(r)$ functions (representing the distribution of interatomic distances in the scattering particles (Svergun et al., 1992), and the dimensionless Kratky plot (informative to check globularity and flexibility of the protein, (Durand et al., 2010, Perez et al., 2001) also showed noteworthy differences, notably a different shoulder at low q on the dimensionless Kratky plot for apo and AMPPNP-bound forms (Figure 3B). Overall, the calculated f/f_0 , R_g , D_{max} indicated that the presence of AMPPNP induces noticeable structural changes making the enzyme more compact (Table S2). Furthermore, deletion of the C-loop promotes slight differences in the scattering curves (Figure 3A). The analysis of the $P(r)$ functions and Kratky plots for GyrBA57 $_{\Delta C-loop}$ showed that in solution the protein adopts features coming from either apo or AMPPNP-bound states (Figures 3B), indicating an intermediate open N-gate conformation.

To further understand these changes, SAXS data were modeled, starting from the atomic coordinates of the extremely open N-gate structures of GyrBA57 (current study) or from the GyrBA57 $_{Nc}$ and GyrBA57 $_{No}$ models using CRY SOL (Figure 3C,D) (Svergun et al., 1995). None of the experimental data did fit the two open nor the closed conformations for GyrBA57 apo state (Figure 3C and Table S1) in line with the analytical ultracentrifugation data. However, the experimental data of the AMPPNP-

bound state (Figure 3D) were close to the expected value of the GyrBA57_{No} model (CRY SOL $\chi^2_{(\text{GyrBA57No model})} = 24.4$ - Table S1) showing that the proposed arrangement of this model was close to the conformation of the AMPPNP-bound state. Using Dadimodo (Roudenko et al., 2018), we adjusted the calculated scattering profile against experimental SAXS data by allowing the reorientation of the ATPase domains with respect to the rest of the structure. The theoretical sedimentations of 15 of the best apo state Dadimodo models were in good agreement with the experimental values (varying between 8.7 and 8.9 S for the models which is comparable to the experimental value of 8.8 S). Similarly, the theoretical sedimentations of 8 Dadimodo models of the holo state were in good agreement with the experimental values (varying between 9.4 and 9.5 S for the models with an experimental value of 9.6 S). An example of one of the 15 or 8 best fits for the apo state ($\chi^2=3.1$) and holo state ($\chi^2=1.4$) (Table S1) and their corresponding models is shown in Figure 3A,E-F and S2E-F, respectively. These data confirm that the SAXS model is a good illustration of the open conformations possibly adopted in solution and point to the existence of two different types of opening in presence or absence of AMPPNP (Figure 3E-F and S2E,F). The noisy scattering data preclude the generation of a better Dadimodo model for GyrBA57 Δ C-loop (Figure 3 A). Nevertheless, the model confirms that the protein probably adopts an intermediate N-gate open conformation with theoretical S values (9 S) identical to the expected value.

ATPase domain

Mtb GyrBA57 was crystallized in absence or presence of non-hydrolyzable ATP analog, revealing that the N-gate is open in both structures (Figure 1B-C), implying

that the ATPase domains are not associated to each other even in the presence of nucleotide. The ATP-lid region (residues 104-125) and the side chain of the conserved switch lysine that protrudes from the transducer (Lys372 in *Mtb* DNA gyrase) were largely disordered in both structures, leading to an incomplete ATP-binding site. The four ATPase domains possess a very similar structure (r.m.s.d. about 0.6 Å for 315 C_α atoms) and adopt the RelaxT conformation as previously observed for *Mtb* ATPase domain (Agrawal et al., 2013) (Figure 1C).

In the apo form, the two GyrB N-terminal domains (residues 1 to 430) linked to the GyrB Toprim domains are lying on each side of the cleavage core domain, fully exposing the G-segment binding cavity to the solvent (Figure 1B). The ATPase GHKL subdomains (residues 25-255) are oriented in direction of the C-gate and thus are in direct interaction with their own BRD and Toprim domains (this conformation is stabilized by several salt bridges and hydrogen bonds, Figure S3A-B and Table S3). Furthermore, the ATPase transducer subdomains (residues 255-431) are sitting on the top of the DNA-gate, thus leading to an ATPase domain almost parallel to the two-fold axis of the cleavage core (Figure 1B-C). The two long C-terminal α-helices of this domain are located on the DNA-gate, separated by a distance of nearly 50 Å, parallel to each other and to the G-segment binding cavity (Figure 1B-C). In the AMPPNP-bound form, the two GyrB ATPase domains lie in a position similar to the position found in the apo form. The superposition of the apo and holo structures reveals a slight nucleotide-induced movement of the ATPase domains leading to a larger N-gate opening for the holoenzyme (Figure 1C), whereas both cleavage cores display a similar global organization (r.m.s.d. of 0.8 Å over 1231 C_α atoms). There was clear density for the two AMPPNP molecules, which exhibit the same conformation in both subunits of the asymmetric unit (Figure S3C). An Mg²⁺ ion is

coordinated by α - and γ -phosphates, one main-chain nitrogen and side-chain interactions with Glu48 and Asn52. There is no interaction with the switch lysine (too far away from the binding cavity) and residues from the ATP-lid.

Interestingly, the flexible linker connecting the ATPase domain (residues 1-426) to the Toprim domain (residues 454-675) is clearly visible in the apo structure. This 25-residues mobile loop, which bridges a distance of 26 Å (Figure S4A), allows for pivoting and dimerization of GyrB domains necessary for N-gate closure.

C-loop

In the crystal structure, the *Mtb* DNA gyrase conformation exhibits an unexpected contact between the ATPase GHKL subdomain and the Toprim/BRD domains (Figure 1 and Figure 4) mediated by the *Corynebacteriales*-specific C-loop (residues 214-245) localized between the last two beta-strands of this domain. Extensive BLAST searches showed that all organisms from the order *Corynebacteriales*, which include notably *Mycobacterium*, *Nocardia*, *Rhodococcus*, *Gordonia*, and *Corynebacterium*, possess a C-loop of about 30-35 amino acids in their ATPase domain (Figure 4B and Figure S5). The amino acid sequence of the C-loop is somewhat variable but its acidic composition (up to one third of acidic residues) is conserved among the *Corynebacteriales* order. In our crystal structures, the peptide chain is well-defined in the electron density for one protomer (Table S3). These results suggest that the C-loop contact region from the BRD includes the ²¹¹DEEE²¹⁴-loop, a motif localized at the solvent-exposed surface of the tower domain in the α 10-loop- α 10' region that creates an extension of the α 10' helix in *Mtb* DNA gyrase (Piton et al., 2010). BLAST searches showed that residues 211 to 214 in GyrA (numbered 1211 to 1214 in our structures) composing this motif are found only

in bacterial GyrA tower domains of *Corynebacteriales* group. The structures indicate that the DEEE-loop acts like a clamp by entangling the C-loop via Van Der Waals contacts (Figure 4C-D), thus illustrating how the two highlighted *Corynebacteriales*-specific motifs (the C- and DEEE-loops) are spatially correlated. Furthermore, the analysis of crystal contacts using PISA (Krissinel and Henrick, 2007) suggest that this interaction is not driven by crystal packing (Figure S6).

Role of the C-loop in DNA gyrase activities and DNA binding

To further investigate the role of the C-loop in the modulation of *Mtb* DNA gyrase activities, we produced several mutants (defined in Figure 1A). The first mutant is a deletion of the entire C-loop (32 amino acids), the others mutants are a combination of selective charge reversal mutations in the C-loop or in the DEEE-loop. The GyrBA_{mC-loop} mutant combined five charge reversal mutation of residues in the C-loop (substitutions details are in Figure 1A legend). The GyrBA_{KKKK} mutant is the charge reversal mutation of all the acidic residues composing the DEEE-loop into basic ones (²¹¹DEEE²¹⁴ into ²¹¹KKKK²¹⁴). Since the catalytic constants for the ATPase activity are the same for the non-fused (gyrase homotetramer) and fused (GyrBA fusion) proteins (Figure S7A), all the experiments were performed on the fused proteins. We investigated the ATPase activity of the wild type (GyrBA - WT), GyrBA_{ΔC-loop}, GyrBA_{mC-loop}, and GyrBA_{KKKK} using a PK/LDH (pyruvate kinase/lactate dehydrogenase)-linked enzyme assay in which ATP hydrolysis is linked to the oxidation of NADH to NAD⁺ (Lindsley, 2001). Firstly, comparison of the catalytic constants obtained for the WT enzyme (Table 2) with the values observed for *E. coli* DNA gyrase ($K_M = 830 \mu\text{M}$ and $k_{cat} = 1.2 \text{ s}^{-1}$) (Gross et al., 2003), indicated a K_M value almost similar for the two enzymes but a 24-fold decrease of k_{cat} pointing to a

reduced ATPase catalytic efficacy for *Mtb* gyrase. Deletion of the C-loop mainly affected the k_{cat} value of GyrBA $_{\Delta C-loop}$, resulting in a 2-fold increase (Figure 5A and Table 2). No significant variation was found for the two GyrBA57 enzymes (Table 2). In contrast, whereas DNA stimulates ATPase activity of WT gyrase by more than 20-fold following a classical dose-response effect (data not shown), it stimulates GyrBA $_{\Delta C-loop}$ ATPase activity by only 6-fold (Figure 5B). Furthermore, mutants of the C-loop (GyrBA $_{mC-loop}$) and DEEE-loop (GyrBA $_{KKKK}$) were found to have the same effect on the ATPase activity, namely a 2-fold increase of the k_{cat} value and a lower boost of ATPase activity in the presence of DNA. The above results confirm the role of these two specific motifs in the low ATPase activity of *Mtb* gyrase (Figure 5A-B and Table 2).

We then tested the effect of the ΔC -loop mutation on DNA strand passage. As no knock down in activity was observed between the non-fused and fused proteins (Figure S7B), we used again the fused proteins for these experiments. Negative DNA supercoiling specific activities were not significantly different between WT and ΔC -loop gyrases (triplicate experiments led to mean values of $2 \cdot 10^5$ and $1.5 \cdot 10^5$ U/mg, respectively) (Figure 5C). Similar results were also observed for DNA decatenation (data not shown), confirming that the mutation has little effect on DNA strand passage despite clear impact on basal ATPase rate (e.g. in absence of DNA).

We next questioned whether the C-loop affects DNA binding. GyrBA57 or C-loop-deleted GyrBA57 gyrases were incubated with a fluorescein-labeled 50-bp duplex oligonucleotide and their binding activities were assessed using electrophoretic mobility shift assays (EMSAs). We found that the C-loop-deleted gyrase keeps its capacity of binding small DNA fragment and we observed a shift of migration between the apo and DNA-bound forms (Figure 5D, right panel). This mobility shift

might be related to a specific gyrase conformation stabilized by the binding of DNA, though we cannot exclude a migrating effect due to the change in charge that results from the ablation of the highly electronegative C-loop.

DISCUSSION

The structural organization of fully functional type IIA topoisomerases has been elucidated only for two enzymes, the yeast topo II (Schmidt et al., 2012) and the *S. pneumoniae* topo IV (Laponogov et al., 2013) (Figure 2A). The work described here fills a gap, providing structural insights into domain organization and inter-domain linkers of a DNA gyrase. Comparison of the two open N-gate structures, *Mtb* gyrase (this work) and *S. pneumoniae* topo IV (Laponogov et al., 2013), reveals a totally different N-gate opening, which represents a specific snapshot of this type II topoisomerase. The *Mtb* gyrase open state observed in the absence and presence of AMPPNP, is an “extremely open” N-gate state since the two GHKL domains are totally stuck to each BRD from the same protomer (Figure 1C and Figure 2B). The surprising result is its persistence even in the presence of AMPPNP, in apparent contradiction with previous structural studies on other topoisomerases reporting that ATP binding within a subunit promotes a reordering of structural elements that favors dimerization of these domains and thus the closing of the N-gate even in the absence of DNA (Wigley et al., 1991, Classen et al., 2003, Bellon et al., 2004, Gubaev and Klostermeier, 2011, Göttler and Klostermeier, 2007). Our results indicate that this open conformation for *Mtb* gyrase is stable enough to be crystallized and our SAXS studies also show that an N-gate open conformation persists in solution even after several days of incubation with the ATP analogue (Figure 3). Furthermore, the GyrBA57 structure confirms the RelaxT conformation, intermediate between the

previously observed RelaxED and ATP-restrained (Corbett and Berger, 2005, Agrawal et al., 2013) conformations, found for the isolated *Mtb* ATPase domain in complex with AMPPCP (Agrawal et al., 2013). In addition, we solved a structure of a topoisomerase-nucleotide complex free of DNA suggesting that ATP binding can precede DNA binding but DNA-binding is necessary to speed up the closing of the N-gate. Since we show that this extremely open N-gate conformation is stabilized through polar interactions and salt bridges, including those between the C- and the DEEE-loops that bring spatially together the two *Corynebacteriales* specific motifs (Figure 4C).

The link between DNA binding and ATP turnover still remains one of the most mysterious aspects of type II topoisomerase activity. An interesting feature of the *Mtb* DNA gyrase structures reported here is the C-loop-mediated connection between the ATPase GHKL subdomain and the cleavage core (Figure 1 and Figure 4). Deletion or modification of this 32-amino acids insert has a clear impact on basal ATP hydrolysis suggesting that this “extremely open” conformation corresponds to a resting state of the enzyme (Table 2). In this state, *Mtb* gyrase hydrolyses less ATP giving the bacteria the opportunity to save energy. On the other hand, the C-loop deletion has no significant effect on DNA binding of short DNA (Figure 5D). This observation correlates well with the lack of contacts between the C-loop and a modelled G-segment (21 bp) DNA as observed in a co-crystal structure with *Mtb* cleavage core gyrase (Blower et al., 2016) (Figure S4B). For the binding of longer DNA, we show that the DNA-stimulated ATPase activity was lower for the mutants that affect C-loop interactions, suggesting that this motif plays an indirect role in the connection between DNA binding and ATP turnover. Interestingly, this goes in the same way than the small differences we observed for negative supercoiling activities.

The highly biased composition (A/E/D-rich) and sparse conservation of the C-loop throughout the *Corynebacteriales* DNA gyrases sequences together with the fact that it gets ordered when it contacts other gyrase domains confirm the mainly structural role for this insert. Whereas the C-loop is highly specific to one order of the class Actinobacteria, the *Corynebacteriales* (Figure 4B and Figure S5), another insert of 170-amino acids, more widely spread, has been described in the Toprim domain of GyrB from several phyla, including proteobacteria, acidobacteria, chlamydia and aquificae (Schoeffler et al., 2010). Structural and functional studies on *E. coli* gyrase revealed that this insert has two functions, acting as a steric buttress to pre-configure the primary DNA-binding site, and serving as a relay that may help coordinate communication between different functional domains (Schoeffler et al., 2010). In *Mtb* gyrase, this GyrB insert is absent but the C-loop has a structural role in the communication between the functional domains. An almost similar role was shown for the residues corresponding to the very C-terminal end of the N-terminal ATPase domain of the human topoisomerase II α (named K-loop by (Schmidt et al., 2012) due to the presence of six consecutive lysines). Indeed, Bjergbaek et al. showed that this highly conserved region is essential for correct two-way communication between the N-terminal and central cleavage/religation domains in eukaryotic topoisomerase II (Bjergbaek et al., 2000). Schmidt *et al.* confirmed the role of this lysine-rich region in the yeast topo II and they showed that this K-loop contacts the ends of a 30 bp DNA duplex (Schmidt et al., 2012). In gyrase enzymes, this motif is not so clearly defined. Indeed, the structurally equivalent loop contains several lysine residues, but is longer than the one found in eukaryotic topo II and the lysines are not consecutive (4 in *Mtb* gyrase). In summary, the C- and K-loops are not implicated in the same type of interactions but both have a critical role for ATP hydrolysis

The features revealed by our work together with available partial structures led us to propose original insights into *Mtb* DNA gyrase nucleotide binding and DNA capture and transport, potentially extendable to *Corynebacteriales* (Figure 6). Our work highlights the existence of *Mtb* DNA gyrase specific resting states. The first one corresponds to the enzyme in absence of DNA and nucleotide with an “extremely open” N-gate, stable enough to be characterized in the crystal and in solution. The second one corresponds to the enzyme after nucleotide binding but before DNA binding. These open conformations of the N-gate, e.g. ATPase domains in their non-dimeric form, allows for the unhindered approach of the G-segment DNA (Figure 6). The open N-gate conformation observed for the AMPPNP-bound *Mtb* gyrase was also observed for the DNA-bound pneumococcal topo IV structure (Figure 6, Laponogov et al., 2013). These results suggest that the simultaneous binding of ATP and DNA is needed to speed up the ATPase domains conformational changes necessary to lock the N-gate. For *Mtb* gyrase, if ATP firstly binds, the approach of the DNA segments will destabilize more rapidly the interactions between the C-loop and the cleavage core and thus the ATPase domains filled with two ATP and sensing the presence of both the T- and G-segments can undergo several rearrangements allowing the enzyme to escape from its resting state. The switch-lysine loop, the ATP-lid and the N-terminal arm of GyrB form a complete ATP-binding site, thus locking the dimerized ATPase domains together with the T-segment inside. To reach the closed conformation observed for the GyrBA57_{Nc} model, the ATPase domains must undergo a large conformational movement of nearly 160 Å with a double 180° rotations around the extreme C-terminal of the last ATPase domain helix (Figure S2C). The following steps of the catalytic cycle are similar to what has been already described for other type II topoisomerases (Lindsley and Wang, 1993, Vos et al.,

2011, Berger et al., 1996, Nitiss, 2009). Induced by ATPase subunits dimerization and T-segment capture, the G-segment is then cleaved and ATP hydrolysis, strand passage and resealing of the G-segment follow. Finally, the C-gate opens, the T-segment exits the protein through the C-gate and the cycle is completed.

In conclusion, this study has revealed the domain connections and organization at high resolution of a gyrase (full-length GyrB-GyrA57)₂ as well as the existence of a specific *Corynebacteriales* gyrase connection between the N-gate and the cleavage core of the enzyme via the two specific motifs, i.e. the C- and DEEE-loops. We have shown that *Mtb* enzyme has a low basal ATPase activity in agreement with previous studies (Agrawal et al., 2013, Tretter and Berger, 2012), which can be explained by the stabilization of the N-gate in an open conformation by this specific connection. Furthermore, the presence of this C-loop indirectly slightly modulates the DNA-stimulated ATPase activity of *Mtb* DNA gyrase and has little impact on DNA strand passage. This modulation could in part explain why the N-gate region is essential in recognition of DNA geometry by *Mtb* gyrase as it was highlighted very recently (Ashley et al., 2017). Therefore, our observations strengthen the idea that *Mtb* DNA gyrase must escape from the “extremely open” N-gate conformation before it can proceed onto the productive catalytic pathway, it does explain the lower ATPase activity of *Mtb* gyrase compared to gyrase (Gross et al., 2003) without C-loop motif and this motif probably plays a role in the regulation for optimal level of gyrase activity in *Mtb* and related bacteria.

Future work is necessary to investigate the potential implication of the C-loop in specific interactions with gyrase regulatory proteins and the ability of the inter domains linkers as specific targets for novel therapies focusing on the conformational movements of *Mtb* gyrase.

ACKNOWLEDGEMENTS

The authors are grateful to Ahmed Haouz, Patrick Weber and Cedric Pissis for performing robot-driven crystallization trials. They also acknowledge the synchrotron sources ESRF more particularly ID29 and BM29 beamlines (Grenoble, France) and SOLEIL ESRF more particularly SWING and PX2 (Saclay, France) for granting access to their facilities and we thank the staff for constant support and help. They thank Sebastien Brule and Bruno Baron for performing AUC and CD experiments. They thank Pierre Roblin and Marc Nadal for helpful discussions. This work was partially supported by grants from Institut Pasteur, Université Paris Diderot and Sorbonne-Université (France).

AUTHOR CONTRIBUTIONS

A.A., C.M. and S.P. designed and supervised the studies. E.C. performed and analyzed the gyrase activity assays. S.P. designed, performed and analyzed the crystallographic study, ATPase activity tests and DNA-binding assays with the help of C.G. P.M.A. participated to the refinement of the structural models. B.R. performed and analyzed the SAXS experiments with the help of A.T. for the Dadimodo analysis. F.B. contributed to the analysis of the SAXS data. C.M. and S.P. wrote the manuscript with input from all the authors, A.A. and P.M.A. contributed to the reading of the manuscript.

DECLARATION OF INTERESTS

The authors declare no competing interests.

REFERENCES

- Adams, P.D., Afonine, P.V., Bunkóczi, G., Chen, V.B., Davis, I.W., Echols, N., Headd, J.J., Hung, L.-W., Kapral, G.J., Grosse-Kunstleve, R.W., McCoy, A.J., Moriarty, N.W., Oeffner, R., Read, R.J., Richardson, D.C., Richardson, J.S., Terwilliger, T.C., Zwart, P.H. (2010). PHENIX: a comprehensive Python-based system for macromolecular structure solution. *Acta Crystallogr. D Biol. Crystallogr.* **66**, 213–221.
- Agrawal, A., Roué, M., Spitzfaden, C., Petrella, S., Aubry, A., Hann, M., Bax, B., Mayer, C. (2013). Mycobacterium tuberculosis DNA gyrase ATPase domain structures suggest a dissociative mechanism that explains how ATP hydrolysis is coupled to domain motion. *Biochem. J.* **456**, 263–273.
- Ashley, R.E., Blower, T.R., Berger, J.M., Osheroff, N. (2017). Recognition of DNA Supercoil Geometry by Mycobacterium tuberculosis Gyrase. *Biochemistry* **56**, 5440–5448.
- Aubry, A., Mark Fisher, L., Jarlier, V., Cambau, E. (2006). First functional characterization of a singly expressed bacterial type II topoisomerase: The enzyme from Mycobacterium tuberculosis. *Biochemical and Biophysical Research Communications* **348**, 158–165.
- Baker, N.M., Weigand, S., Maar-Mathias, S., Mondragon, A. (2010). Solution structures of DNA-bound gyrase. *Nucleic Acids Research* **39**, 755–766.
- Bax, B.D., Chan, P.F., Eggleston, D.S., Fosberry, A., Gentry, D.R., Gorrec, F., Giordano, I., Hann, M.M., Hennessy, A., Hibbs, M., Huang, J., Jones, E., Jones, J., Brown, K.K., Lewis, C.J., May, E.W., Saunders, M.R., Singh, O., Spitzfaden, C.E., Shen, C., Shillings, A., Theobald, A.J., Wohlkonig, A., Pearson, N.D., Gwynn, M.N. (2010). Type IIA topoisomerase inhibition by a new class of antibacterial agents. *Nature* **466**, 935–940.
- Bellon, S., Parsons, J.D., Wei, Y., Hayakawa, K., Swenson, L.L., Charifson, P.S., Lippke, J.A., Aldape, R., Gross, C.H. (2004). Crystal structures of Escherichia coli topoisomerase IV ParE subunit (24 and 43 kilodaltons): a single residue dictates differences in novobiocin potency against topoisomerase IV and DNA gyrase. *Antimicrob. Agents Chemother.* **48**, 1856–1864.
- Berger, J.M., Gamblin, S.J., Harrison, S.C., Wang, J.C. (1996). Structure and mechanism of DNA topoisomerase II. *Structure and mechanism of DNA topoisomerase II.* **379**, 225–232.
- Bjergbaek, L., Kingma, P., Nielsen, I.S., Wang, Y., Westergaard, O., Osheroff, N., Andersen, A.H. (2000). Communication between the ATPase and cleavage/religation domains of human topoisomerase IIalpha. *J. Biol. Chem.* **275**, 13041–13048.
- Blower, T.R., Williamson, B.H., Kerns, R.J., Berger, J.M. (2016). Crystal structure and stability of gyrase-fluoroquinolone cleaved complexes from Mycobacterium tuberculosis. *Proc. Natl. Acad. Sci. U.S.A.* **113**, 1706–1713.
- Bouige, A., Darmon, A., Piton, J., Roué, M., Petrella, S., Capton, E., Forterre, P., Aubry, A., Mayer, C. (2013). Mycobacterium tuberculosis DNA gyrase possesses two functional GyrA-boxes. *Biochem. J.* **455**, 285–294.
- Classen, S., Olland, S., Berger, J.M. (2003). Structure of the topoisomerase II ATPase region and its mechanism of inhibition by the chemotherapeutic agent ICRF-187. *Proc. Natl. Acad. Sci. U.S.A.* **100**, 10629–10634.
- Cole, S.T., Brosch, R., Parkhill, J., Garnier, T., Churcher, C., Harris, D., Gordon, S.V., Eiglmeier, K., Gas, S., Barry, C.E., Tekaiia, F., Badcock, K., Basham, D., Brown,

- D., Chillingworth, T., Connor, R., Davies, R., Devlin, K., Feltwell, T., Gentles, S., Hamlin, N., Holroyd, S., Hornsby, T., Jagels, K., Krogh, A., McLean, J., Moule, S., Murphy, L., Oliver, K., Osborne, J., Quail, M.A., Rajandream, M.A., Rogers, J., Rutter, S., Seeger, K., Skelton, J., Squares, R., Squares, S., Sulston, J.E., Taylor, K., Whitehead, S., Barrell, B.G. (1998). Deciphering the biology of *Mycobacterium tuberculosis* from the complete genome sequence. *Nature* **393**, 537–544.
- Corbett, K.D., Berger, J.M. (2005). Structural Dissection of ATP Turnover in the Prototypical GHF ATPase TopoVI. *Structure* **13**, 873–882.
- Corbett, K.D., Berger, J.M. (2004). Structure, Molecular Mechanisms, and Evolutionary Relationships in DNA Topoisomerases. *Annual Review of Biophysics and Biomolecular Structure* **33**, 95–118.
- Costenaro, L., Grossmann, J.G., Ebel, C., Maxwell, A. (2005). Small-Angle X-Ray Scattering Reveals the Solution Structure of the Full-Length DNA Gyrase A Subunit. *Structure* **13**, 287–296.
- Cove, M.E., Tingey, A.P., Maxwell, A. (1997). DNA gyrase can cleave short DNA fragments in the presence of quinolone drugs. *Nucleic Acids Research* **25**, 2716–2722.
- Darmon, A., Piton, J., Roué, M., Petrella, S., Aubry, A., Mayer, C. (2012). Purification, crystallization and preliminary X-ray crystallographic studies of the *Mycobacterium tuberculosis* DNA gyrase CTD. *Acta Crystallogr. Sect. F Struct. Biol. Cryst. Commun.* **68**, 178–180.
- Durand, D., Vivès, C., Cannella, D., Perez, J., Pebay-Peyroula, E., Vachette, P., Fieschi, F. (2010). NADPH oxidase activator p67(phox) behaves in solution as a multidomain protein with semi-flexible linkers. *J. Struct. Biol.* **169**, 45–53.
- Emsley, P., Lohkamp, B., Scott, W.G., Cowtan, K. (2010). Features and development of Coot. *Acta Crystallogr. D Biol. Crystallogr.* **66**, 486–501.
- Evrard, G., Mareuil, F., Bontems, F., Sizun, C., Perez, J. (2011). DADIMODO: a program for refining the structure of multidomain proteins and complexes against small-angle scattering data and NMR-derived restraints. *J Appl Crystallogr* **44**, 1264–1271.
- Fu, G., Wu, J., Liu, W., Zhu, D., Hu, Y., Deng, J., Zhang, X.-E., Bi, L., Wang, D.-C. (2009). Crystal structure of DNA gyrase B' domain sheds lights on the mechanism for T-segment navigation. *Nucleic Acids Research* **37**, 5908–5916.
- Göttler, T., Klostermeier, D. (2007). Dissection of the nucleotide cycle of *B. subtilis* DNA gyrase and its modulation by DNA. *367*, 1392–1404.
- Gross, C.H., Parsons, J.D., Grossman, T.H., Charifson, P.S., Bellon, S., Jernee, J., Dwyer, M., Chambers, S.P., Markland, W., Botfield, M., Raybuck, S.A. (2003). Active-site residues of *Escherichia coli* DNA gyrase required in coupling ATP hydrolysis to DNA supercoiling and amino acid substitutions leading to novobiocin resistance. *Antimicrob. Agents Chemother.* **47**, 1037–1046.
- Gubaev, A., Klostermeier, D. (2011). DNA-induced narrowing of the gyrase N-gate coordinates T-segment capture and strand passage. *Proc. Natl. Acad. Sci. U.S.A.* **108**, 14085–14090.
- Kabsch, W. (2010). Integration, scaling, space-group assignment and post-refinement. *66*, 133–144.
- Karplus, P.A. and Diederichs, K. (2012). Linking Crystallographic Model and Data Quality. *Science*. **336**, 1030–1033.
- Kirchhausen, T., Wang, J.C., Harrison, S.C. (1985). DNA gyrase and its complexes with DNA: direct observation by electron microscopy. *Cell* **41**, 933–943.

- Konarev, P.V., Volkov, V.V., Sokolova, A.V., Koch, M.H.J., Svergun, D.I. (2003). PRIMUS: a Windows PC-based system for small-angle scattering data analysis. *J Appl Crystallogr* 36, 1277–1282.
- Krissinel, E., Henrick, K. (2007). Inference of Macromolecular Assemblies from Crystalline State. *J. Mol. Biol.* 372, 774–797.
- Lanz, M.A., Klostermeier, D. (2011). Guiding strand passage: DNA-induced movement of the gyrase C-terminal domains defines an early step in the supercoiling cycle. *Nucleic Acids Research* 39, 9681–9694.
- Laponogov, I., Veselkov, D.A., Crevel, I.M.T., Pan, X.S., Fisher, L.M., Sanderson, M.R. (2013). Structure of an “open” clamp type II topoisomerase-DNA complex provides a mechanism for DNA capture and transport. *Nucleic Acids Research* 41, 9911–9923.
- Levine C, Hiasa H, Marians KJ (1998). DNA gyrase and topoisomerase IV: biochemical activities, physiological roles during chromosome replication, and drug sensitivities. *Biochim Biophys Acta* 1400: 29–43.
- Lindsley, J.E. (2001). Use of a real-time, coupled assay to measure the ATPase activity of DNA topoisomerase II. *Methods Mol. Biol.* 95, 57–64.
- Lindsley, J.E., Wang, J.C. (1993). Study of allosteric communication between protomers by immunotagging. *Nature* 361, 749–750.
- Mareuil, F., Sizun, C., Perez, J., Schoenauer, M., Lallemand, J.-Y., Bontems, F. (2007). A simple genetic algorithm for the optimization of multidomain protein homology models driven by NMR residual dipolar coupling and small angle X-ray scattering data. *Eur. Biophys. J.* 37, 95–104.
- McCoy, A.J., Grosse-Kunstleve, R.W., Adams, P.D., Winn, M.D., Storoni, L.C., Read, R.J. (2007). Phaser crystallographic software. *J Appl Crystallogr* 40, 658–674.
- Nitiss, J.L. (2009). DNA topoisomerase II and its growing repertoire of biological functions. *9*, 327–337.
- Ortega, A., Amorós, D., García de la Torre, J. (2011). Prediction of hydrodynamic and other solution properties of rigid proteins from atomic- and residue-level models. *Biophys. J.* 101, 892–898.
- Painter, J., Merritt, E.A. (2006). Optimal description of a protein structure in terms of multiple groups undergoing TLS motion. *62*, 439–450.
- Papillon, J., Ménétret, J.-F., Batisse, C., Hélye, R., Schultz, P., Potier, N., Lamour, V. (2013). Structural insight into negative DNA supercoiling by DNA gyrase, a bacterial type 2A DNA topoisomerase. *Nucleic Acids Research* 41, 7815–7827.
- Pérez, J., Vachette, P., Russo, D., Desmadril, M., Durand, D. (2001). Heat-induced unfolding of neocarzinostatin, a small all-beta protein investigated by small-angle X-ray scattering. *J. Mol. Biol.* 308, 721–743.
- Piton, J., Matrat, S., Petrella, S., Jarlier, V., Aubry, A., Mayer, C. (2009). Purification, crystallization and preliminary X-ray diffraction experiments on the breakage-reunion domain of the DNA gyrase from *Mycobacterium tuberculosis*. *Acta Crystallogr. Sect. F Struct. Biol. Cryst. Commun.* 65, 1182–1186.
- Piton, J., Petrella, S., Delarue, M., André-Leroux, G., Jarlier, V., Aubry, A., Mayer, C. (2010). Structural insights into the quinolone resistance mechanism of *Mycobacterium tuberculosis* DNA gyrase. *PLoS ONE* 5, e12245.
- Rogé, J., and Betton, J.M. (2005). Use of pIVEX plasmids for protein overproduction in *Escherichia coli*. *Microb. Cell Fact.* 4, 18.
- Roudenko O., Thureau A., Perez J. (2018). Dadimodo, Refining Atomic MultiDomain Proteins against SAXS Data (<https://dadimodo.synchrotron-soleil.fr>).

- Roué, M., Agrawal, A., Volker, C., Mossakowska, D., Mayer, C., Bax, B.D. (2013). Purification, crystallization and preliminary X-ray crystallographic studies of the *Mycobacterium tuberculosis* DNA gyrase ATPase domain. *Acta Crystallogr. Sect. F Struct. Biol. Cryst. Commun.* **69**, 679–682.
- Schmidt, B.H., Osheroff, N., Berger, J.M. (2012). Structure of a topoisomerase II-DNA-nucleotide complex reveals a new control mechanism for ATPase activity. *Nat. Struct. Mol. Biol.* **19**, 1147–1154.
- Schoeffler, A.J., Berger, J.M. (2008). DNA topoisomerases: harnessing and constraining energy to govern chromosome topology. *Q. Rev. Biophys.* **41**, 41–101.
- Schoeffler, A.J., May, A.P., Berger, J.M. (2010). A domain insertion in *Escherichia coli* GyrB adopts a novel fold that plays a critical role in gyrase function. *Nucleic Acids Research* **38**, 7830–7844.
- Svergun, D., Barberato, C., Koch, M.H.J. (1995). CRY SOL— a Program to Evaluate X-ray Solution Scattering of Biological Macromolecules from Atomic Coordinates. *J Appl Crystallogr* **28**, 768–773.
- Svergun, D.I. (1992). Determination of the regularization parameter in indirect-transform methods using perceptual criteria. *J Appl Crystallogr* **25**, 495–503.
- The PyMOL Molecular Graphics System, Version 1.8 Schrödinger, LLC, n.d. The PyMOL Molecular Graphics System, Version 1.8 Schrödinger, LLC.
- Tretter, E.M., Berger, J.M. (2012). Mechanisms for defining supercoiling set point of DNA gyrase orthologs: II. The shape of the GyrA subunit C-terminal domain (CTD) is not a sole determinant for controlling supercoiling efficiency. *J. Biol. Chem.* **287**, 18645–18654.
- Tretter, E.M., Schoeffler, A.J., Weisfield, S.R., Berger, J.M. (2010). Crystal structure of the DNA gyrase GyrA N-terminal domain from *Mycobacterium tuberculosis*. *Proteins* **78**, 492–495.
- Vos, S.M., Tretter, E.M., Schmidt, H.B., Berger, J.M. (2011). All tangled up: how cells direct, manage and exploit topoisomerase function. *12*, 827–841.
- Wigley, D.B., Davies, G.J., Dodson, E.J., Maxwell, A., Dodson, G. (1991). Crystal structure of an N-terminal fragment of the DNA gyrase B protein. *Nature* **351**, 624–629.
- Winn, M.D., Ballard, C.C., Cowtan, K.D., Dodson, E.J., Emsley, P., Evans, P.R., Keegan, R.M., Krissinel, E.B., Leslie, A.G.W., McCoy, A., McNicholas, S.J., Murshudov, G.N., Pannu, N.S., Potterton, E.A., Powell, H.R., Read, R.J., Vagin, A., Wilson, K.S. (2011). Overview of the CCP4 suite and current developments. *67*, 235–242.
- Wohlkonig, A., Chan, P.F., Fosberry, A.P., Homes, P., Huang, J., Kranz, M., Leydon, V.R., Miles, T.J., Pearson, N.D., Perera, R.L., Shillings, A.J., Gwynn, M.N., Bax, B.D. (2010). Structural basis of quinolone inhibition of type IIA topoisomerases and target-mediated resistance. *17*, 1152–1153.

FIGURE TITLES AND LEGENDS

Figure 1. High-resolution ‘open clamp’ structure of *Mtb* DNA gyrase.

(A) Domain organization of the *Mtb* DNA gyrase constructs used in this study.

Functional regions are colored and labelled. The linker connecting the DNA gyrase A and B subunits is represented in a gray dash line (three-amino acid linker: G-D-L). The green insertion in the GHKL domain corresponds to the C-loop (residues 214-245 in GyrB). The white region represented by Δ illustrates the C-loop region deleted in the Δ C-loop mutants. The gray region in the GHKL domain corresponds to the substitution of five residues in the C-loop implicated in salt bridges or strong hydrogen interactions participating to the stabilization of the N-gate extremely open conformation (Figure S3A-B; the five substitutions are: E221K – D225K – E228K – R236E – H244A and the mutant name is GyrBA_{mCloop}). The purple region in the BRD domain (residues 251 to 255) corresponds to the substitution of the DEEE into KKKK residues (named GyrBA_{KKKK}).

(B) Crystal structure of *Mtb* DNA gyrase (apo form). One protomer is gray shaded, one is colored as in A.

(C) Superposition of the apo (colored as in A) and AMPPNP-bound (gray) forms of *Mtb* gyrase (r.m.s.d. value of 1.2 Å for 1719 C α atoms).

Figure 2. ‘Open’ and ‘closed’ N-gate conformations known from crystallographic structures, comparison with the *Mtb* DNA gyrase extremely open N-gate conformation.

(A) ‘closed’ N-gate structure of yeast topo II (PDB 4GFH), ‘open’ N-gate structure of pneumococcal topo IV (PDB 4I3H), ‘extremely open’ N-gate structure of *Mtb* gyrase (current work).

(B) Superposition of *Mtb* gyrase structure (apo form, current structure) and 'open' N-gate structure of pneumococcal topo IV (PDB 4I3H). The enzymes are colored as in Figure 1A, except for the ATPase domain of 4I3H colored in gray.

Figure 3. SAXS studies.

(A) SAXS profiles of *Mtb* gyrase: GyrBA57 apo (open dot), AMPPNP-bound form (incubation with AMPPNP during 6 days – red triangle) and GyrBA57 $_{\Delta C\text{-loop}}$ (orange square). Superposition of the generated Dadimodo models, apo, AMPPNP-bound and $\Delta C\text{-loop}$ in solid line gray, red and orange, respectively.

(B) Dimensionless Kratky plot scattering patterns using the figure 3A color code. Inset: distance distribution functions $P(r)$ derived from the three samples scattering patterns scaled to $I(0)$ obtained using the program GNOM.

(C, D) Theoretical scattering curves from CRY SOL for the various conformation states of GyrBA57 (models manually constructed from the structure of GyrBA57 using the 3D structures of yeast topo II (4GFH) and *pneumococcal* topo IV (4I3H)): closed N-gate model 4GFH model (GyrBA5 $_{Nc}$ - blue), crystal structure of *Mtb* gyrase i.e., "extremely open" N-gate conformation (GyrBA57 - forest green), and open N-gate 4I3H model (GyrBA57 $_{No}$ - purple). Inset representation of open and closed states of *Mtb* gyrase using the figure 3A color code. The longest distances in each structure are indicated. Experimental scattering curve for apo state is represented in open dot. Experimental scattering curve for AMPPNP-bound state is represented in red triangle.

(E, F) Generated Dadimodo model of *Mtb* DNA gyrase. BRD and Toprim domains from GyrBA57 structure are represented in transparent surface colored as in figure 1A. In the two panels, the ATPase domains are represented in cartoon

representation: GyrBA57 in pale yellow, topo IV in light gray, the Dadimodo generated model in dark gray and red for the apo and AMPPNP-bound forms, respectively.

Figure 4. Close-up view on the C-loop.

(A) Close-up view of the C-loop intramolecular interactions. The C-loop is surrounded by 2Fo-Fc electron density map contoured to 1.0σ (blue).

(B) Sequence alignment of *Mtb*, *Nocardia brasiliensis*, *Gordonia paraffinivorans*, *Segniliparus rotundus*, *Tsukamurella paurometabola*, *Corynebacterium resitens*, *Corynebacterium glutamicum*, *E. coli* DNA gyrases, *Streptococcus pneumoniae* topo IV and *Saccharomyces cerevisiae* topo II. The residues corresponding to the C-loop insertion are colored in blue.

(C) Surface representation of the apo structure of *Mtb* gyrase (current work). The DEEE motif is highlighted in gray.

(D) Close-up view of Figure 4C centered on the C- and DEEE-loops.

Figure 5. C- and DEEE-loops mutants have a 2-fold increase of basal ATPase rates but a lower DNA stimulation of ATP hydrolysis.

(A) Basal ATPase activity. Wild-type (WT) GyrBA mutant gyrases activities are plotted as a function of ATP concentration and fit to a standard Michaelis-Menten kinetic model.

(B) DNA-stimulated ATPase activity. Bar chart showing the ATPase activity of WT and GyrBA mutant gyrases activities observed at constant ATP concentration in the absence or presence of DNA. Errors bars, s.e.m. from three independent experiments.

(C) deleted C-loop mutant has a slight decrease in negative DNA supercoiling. Protein concentrations are listed in ng. The gel is representative of triplicate data. Relaxed and supercoiled DNA species are labeled with cartoon representations on the right of the native gel.

(D) DNA binding. Interaction of GyrBA57 and GyrBA57 $_{\Delta C-loop}$ with DNA (50-bp duplex oligonucleotide corresponding to the pBR322 strong gyrase-binding site). The GyrBA57 proteins were used in this assay to avoid competition from the CTD in G-segment binding. Protein is at constant concentration (1 200 nM) and is incubated with 0 nM of DNA (-) or 1 200 nM of DNA (+). The same gel is revealed with UV light (DNA fluorescence signal) and after by staining with Coomassie Blue (proteins). Arrows indicate the positions of free DNA (F) and DNA-protein complex (C).

Figure 6. Proposed model for *Mtb* DNA gyrase nucleotide binding and DNA capture and transport.

Schematic representation of the resting states and the steps of the *Mtb* gyrase catalytic cycle. DNA gyrase is colored as in Figure 1A. The C-loop is marked by a green “loop” (front view) or a green star (90° rotation view), the ATP by a black circle. The C-loop stabilizes an “extremely open” N-gate conformation, observed for the apo form (this state is shown in a front view and a 90° rotation of the protein) and for the DNA-free AMPPNP-bound complex (with two conformations for the opening of the N-gate observed in the crystal structure and the SAXS model). A DNA-bound AMPPNP-free form of pneumococcal topo IV in an open N-gate conformation has already been identified (Topo IV model, 4I3H), suggesting that ATP and DNA are needed to stabilize a dimeric form of the N-gate for topo IIA enzymes. We proposed that the two states of *Mtb* gyrase observed in this study, are resting states allowing

the bacteria to save energy. *Mtb* DNA gyrase has to escape these states to proceed into a productive catalytic pathway resumed to three steps in our model. In the first step, upon DNA (G- and T-segments represented in gray) binding the C-loop connection is disrupted inducing a conformational rearrangement. In the second and the third steps, the N-terminal ATPase domains dimerize and capture the DNA duplex to be transported through the transient break in the G-segment opened by the BRD.

Table 1. X-Ray Data Collection and Refinement Statistics

	GyrBA57	GyrBA57-AMPPNP-Mg ²⁺
PDB ID code	6GAV	6GAU
Beamline	ESRF-ID29	SOLEIL-PX2
Data collection ^a		
Space group	P 2 ₁	P 1
Cell dimensions		
<i>a</i> , <i>b</i> , <i>c</i> (Å)	97.51 157.62 103.50	91.52 96.78 105.79
α , β , γ (°)	90.0, 98.11, 90.0	75.64, 64.44, 65.80
Resolution range (Å) ^b	48.73-2.6 (2.67-2.6)	47.54-3.3 (3.48-3.3)
Total reflections	330 497 (50 295)	177 190 (25 531)
Unique reflections	94 824 (15 065)	44 305 (6 598)
Redundancy	3.48 (3.3)	3.99 (3.8)
Completeness (%)	99.2 (98.3)	98.2 (90.6)
<i>I</i> / σ <i>I</i>	8.9 (1.21)	7 (1.19)
Wilson B-factor	62.41	86.4
R _{meas} (%)	10.4 (125.3)	23.6 (137)
R _{pim} (%)	4.6 (42.5)	12.9 (75.3)
CC _{1/2} ^c	99.5 (53.1)	99 (51)
Refinement		
Resolution (Å)	2.6	3.29
No. reflections	94 491	44 284
R _{work} /R _{free}	0.19/0.23	0.19/0.25
No. atoms		
Protein	17 437	16 808
Ligand/ion	0	64
Water	47	0
R.m.s. deviations		
Bonds lengths (Å)	0.010	0.010
Bonds angles (°)	1.13	1.2
Average B factor (Å ²)	94	100
AMP-PNP	null	2
Mg ²⁺	null	2
Ramachandran statistics (%) ^d		
Favoured regions	95	88
Allowed regions	4	10
Outliers	0	2

^aValues in parentheses are for highest-resolution shell.

^bThe resolution cutoff was selected based on *I*/ σ *I* and CC_{1/2} according to (Karplus and Diederichs, 2012).

^cCC_{1/2} is the percentage of correlation between intensities from random half-datasets.

^dAs defined by MolProbity

- Table 2. Basal ATPase activity of wild-type, GyrBA_{ΔC-loop}, GyrBA_{mC-loop}, GyrBA_{KKKK}, GyrBA57, GyrBA57_{ΔC-loop} gyrases.

□

Enzyme	K_M (μM)	k_{cat} (s^{-1})
GyrBA	700 ± 170	0.05 ± 0.003
GyrBA _{ΔC-loop}	300 ± 73	0.11 ± 0.005
GyrBA _{mC-loop}	700 ± 100	0.08 ± 0.0025
GyrBA _{KKKK}	1000 ± 160	0.09 ± 0.004
GyrBA57	800 ± 90	0.06 ± 0.002
GyrBA57 _{ΔC-loop}	750 ± 70	0.06 ± 0.001

- Errors are SEM from at least three measurements.

STAR Methods

CONTACT FOR REAGENT AND RESOURCE SHARING

Further information and requests for resources and reagents should be directed to and will be fulfilled by the Lead Contact, Stephanie Petrella (stephanie.petrella@pasteur.fr).

EXPERIMENTAL MODEL AND SUBJECT DETAILS

Growth conditions and chemical treatments

All recombinant proteins were expressed in *E. coli* BLI5(DE3) cells (Rogé and Betton, 2005) grown in Miller's Luria Broth base at 37°C shaking at 200 rpm, with protein expression induced at OD₆₀₀= 0.6 with 0.5 mM isopropyl-β-D-thiogalactopyranoside (IPTG) overnight at 20°C with shaking.

Expression plasmids construction

To simplify structural studies of a tetrameric A₂B₂ complex, *Mtb* GyrB and GyrA were fused with a three-amino acid G-D-L linker, following a strategy previously used for *Thermus thermophilus* DNA gyrase (Papillon et al., 2013), and cloned into in pET28a vector producing a GyrB–GyrA fusion protein (GyrBA) with a N-terminal 6-histidine tag upstream of a TEV cleavage site (Novagen). Several constructions based on this one were also done by site directed mutagenesis, i.e. GyrBA57 (entire GyrB fused to GyrA residues 1–502 named GyrA57 because of its molecular weight of 57 kDa), GyrBA_{ΔC-loop} (GyrB deleted of the C-loop corresponding to residues 214-245 and entire GyrA subunits), GyrBA57_{ΔC-loop} (GyrB deleted of the C-loop corresponding to

residues 214-245 and GyrA57 subunits), GyrBA $_{\Delta mC-loop}$ (substitution of five residues in the C-loop : Glu221Lys – Asp225Lys – Glu228Lys – Arg236Glu – His244Ala), GyrBA $_{KKKK}$ (substitution of the $^{211}DEEE^{214}$ motif into $^{211}KKKK^{214}$) (Figure 1A). Plasmids and various mutant synthetic genes were designed and ordered to Genscript.

METHOD DETAILS

Proteins Expression and Purification.

Proteins expression and purification protocols were the same for all the proteins. After overexpression, cells were harvested by centrifugation and resuspended in buffer A500 (20 mM Tris-HCl, pH 7.5, 500 mM NaCl, 5 mM Imidazole, pH 8.0, 5 mM MgCl₂, 1 mM DTT, and 5% (vol/vol) glycerol). For protein purification, protease inhibitors were added after sonication and fraction was clarified by centrifugation. The supernatant was next loaded onto a 5 mL HisTrap HP column and the His-tagged protein was purified applying a linear imidazole gradient using buffer B500 (20 mM Tris-HCl, pH7.5, 500 mM NaCl, 250 mM Imidazole, pH 8.0, 5 mM MgCl₂, 1 mM DTT, and 5% (vol/vol) glycerol). The GyrBA-containing fractions, as verified by SDS-PAGE, were pooled and prior to a second purification step, the 6-His tag in the protein was removed by incubating for 18 hours at 4 °C in the presence of 6-His tagged TEV protease at a 1/40 ratio (w/w) in buffer C80 (10 mM Tris-HCl, pH 7.5, 80 mM NaCl, 1 mM DTT, 1 mM EDTA, 10% Glycerol), followed by separation on a HisTrap HP column in A500, and the flow-through was collected, concentrated, and dialysed two hours in buffer C before loading the fraction onto a Heparin HP column. Proteins were then purified applying a linear NaCl gradient (80 to 1 000 mM). The

GyrBA-containing fractions, as verified by SDS-PAGE, were pooled and the protein was further purified by size-exclusion chromatography on a Superdex 200 column equilibrated in buffer D (20 mM Tris-HCl, pH 7.5, 100 mM KCl, 1 mM DTT, 1 mM EDTA, Glycerol 10%). Peak fractions were pooled and concentrated up to 15 mg/ml, flash-frozen in liquid nitrogen and stored at -80°C. For samples used for crystallography, this protein was dialyzed overnight into buffer E (20 mM Tris-HCl, pH 7.9, 150 mM NaCl and 2.5 mM DTT). Proteins were quantified by using the molar absorption coefficient predicted from the amino acid sequence by the ProtParam tool.

Negative DNA supercoiling activity assays.

Negative DNA supercoiling activity was assayed using relaxed pBR322 DNA as substrate. The assay reaction mixture (30 μ l) contained supercoiling buffer 1X (40 mM Tris-HCl (pH 7.5), 25 mM KCl, 2 mM spermidine, 4 mM DTT, 0.36 mg/ml BSA, 6 mM magnesium acetate, 100 mM KCl, 0.1 mM EDTA, 1 mM ATP (pH 8.0), 300 ng relaxed pBR322 and the tested gyrase at various concentrations. The mixture was incubated for 1 h at 37°C. The reaction was terminated by adding 12 mM EDTA and by incubating at 37°C for 5 min. The reaction was then deproteinized by adding 2 μ l of SDS (2% w/v) and 2 μ l of proteinase K (1 mg/ml) and further incubated for 15 min. Reactions were analyzed by a 5h to 16h electrophoresis at 50 V through 1% agarose gels with a 0.5x TBE running buffer, in a gel which was stained with ethidium bromide (0.5 μ g/ml) after running. Supercoiling activity was assessed by scanning the fluorescence of the bands corresponding to the supercoiled pBR322 DNA the using Molecular Analyst® software (Bio-Rad). One unit of enzyme activity was defined as the minimum amount of gyrase that converted 0.3 μ g of relaxed pBR322 to the supercoiled form in 1 h at 37°C.

ATPase assays.

Wild-type and mutant DNA gyrase ATPase activities were measured by using an established enzyme-coupled assay in which the hydrolysis of ATP to ADP is coupled to the oxidation of NADH to NAD⁺ (Lindsley, 2001). To determine standard kinetic parameters (K_M , k_{cat}), we incubated 500 nM enzyme with 0-8 mM ATP in 100 μ l reactions. Reactions contained 50 mM HEPES pH 7.5, 150 mM potassium acetate, 8 mM magnesium acetate, 5 mM β -mercaptoethanol, 2 mM phosphoenol pyruvate (PEP), 0.16 mM β -nicotinamide adenine dinucleotide (NADH), and an excess of pyruvate kinase and lactate dehydrogenase. Assays were performed at 30°C, with the oxidation of NADH to NAD⁺ monitored by measuring absorbance at 340 nm in a (TECAN SunriseTM, absorbance microplate reader). ATPase rate as a function of [ATP] was fit for K_M and k_{cat} using Michaelis–Menten kinetics in PRISM. DNA stimulation of ATPase activity was measured using assays performed as described, except that the starting concentration of ATP was held constant (0.5 mM), and reactions were supplemented using purified sheared salmon-sperm DNA.

DNA-binding assays.

DNA binding was visualized by electrophoretic mobility shift assays (EMSAs). The DNA substrate for binding was a 50-bp segment of plasmid pBR322 shown previously to contain a strong gyrase-binding site (Cove et al., 1997). Two complementary single-stranded oligos (5'-GCG AGA AGA ATC ATA ATG GGG AAG GCC ATC CAG CCT CGC GTC GCG CAA CG-3'; 5'-/6-FAM/ CGT TGC GCG ACG

CGA GGC TGG ATG GCC TTC CCC ATT ATG ATT CTT CTC GC-3', where 6-FAM indicates the position of a fluorescein label for visualization) were obtained from Eurogentec and individually resuspended in 100 μ l annealing buffer (10 mM Tris-HCl pH 7.5, 50 mM KCl, 5 mM MgCl₂) to almost 500 μ M final concentration. The two oligonucleotides were then combined in equal molar amounts and annealed at 94°C for 2 minutes and gradually cooled. Double-stranded DNA was stored in annealing buffer at -20°C. The various gyrase mutant proteins were tested at 1 200 nM and incubated with 1 200 nM of the labelled double-stranded 50mer for 30 min at room temperature in 25 μ l reactions containing 30 mM Tris-HCl pH 7.5, 2 mM MgCl₂, 6% glycerol, 1 mM DTT. Reactions were loaded directly onto a 6% PAGE.

Crystallization.

Crystallization screenings were carried out using the sitting-drop vapour diffusion method and a Mosquito nanoliter-dispensing crystallization robot (TTP Labtech). Initial crystallization screening of GyrBA57 at 10 mg.ml⁻¹ were run on either lacking ligand or in the presence of 5 mM MgCl₂ plus 2.5 mM AMPPNP, or in the presence of 1 mM AMPPNP plus 8 μ M oligonucleotides (one oligonucleotide previously crystallized with moxifloxacin and *Acinetobacter baumannii* topo IV (Wohlkonig et al., 2010) and the second one previously crystallized with ciprofloxacin (or GSK299423 and RXV) and *Staphylococcus aureus* DNA gyrase (Bax et al., 2010), 10 μ M Moxifloxacin in presence of 5 mM MnCl₂. 600 crystallization conditions were tested for each combination. Crystal screening was also conducted for GyrBA57 $_{\Delta C}$ -loop protein without success. Crystals were only obtained for the apo form of the protein or in the presence of AMPPNP. These little crystals were obtained in several conditions, but only two of them gave crystals suitable for diffraction, one containing

only 25% Ethylene Glycol (EG) and an another one containing 100 mM Sodium Acetate, 100 mM MES pH 6.5 and 30% PEG 400 (for Apo-GyrBA57 and Holo-GyrBA57, respectively). Initial crystal screening to find suitable crystallization conditions was performed at beamlines PX2 at SOLEIL (Paris) and id29 at European Synchrotron Radiation Facility (Grenoble). After extensive optimization of these conditions using among other Additive Screen (Hampton), the best diffracting crystals were obtained in 100 mM Sodium Acetate, 100 mM MES pH 6.5 and 26% PEG 400 and 25% EG, 10 mM MgCl₂ (for Apo-GyrBA57 and AMPPNP-bound GyrBA57, respectively). The use of a microfocus beamline was essential to collect datasets of good quality, indeed diffraction quality varied greatly between crystals, hundreds of crystals were tested to obtain final datasets.

Structure determination and data collection.

Diffraction data were processed with XDS (Kabsch, 2010). AIMLESS from CCP4 (Winn et al., 2011) corroborated space group as P2₁ for the crystal form without AMPPNP, and P1 for the crystal form containing AMPPNP. The two asymmetric units contained two monomers. Initial molecular replacement for the first structure (apo form, space group P2₁) was performed using PHASER (McCoy et al., 2007) within CCP4 (Winn et al., 2011). The search model was constituted of four searching ensembles: the BRD domain (PDB 3IFZ (Piton et al., 2010)), the TOPRIM domain (PDB 3IG0 (Piton et al., 2010)) and the ATPase domain (PDB 3ZKD (Agrawal et al., 2013)) divided into two subdomains (GHKL and Transducer) from the DNA gyrase of *Mtb*. These search models were modified versions of the PDB, with all waters, drug molecules and metals removed. The obtained solution underwent rigid-body refinement using REFMAC from CCP4. The density map was examined in Coot

(Emsley et al., 2010) and the model was built using Coot and iterative rounds of refinements in Buster and PHENIX (Adams et al., 2010) at the end, including the use of TLS parameters (Painter and Merritt, 2006). For PHENIX, before each refinement, the model was prepared using READYSET (Adams et al., 2010). The final model was used as search model for molecular replacement with the second dataset (holo form, space group P1). Final models all have favorable R / R_{free} values, Molprobity scores and excellent geometry and stereochemistry. The Molprobity overall scores for PDB 6GAV and PDB 6GAU are 1.74 (100%) and 1.14 (100%), respectively. Structure determination statistics are provided in Table 1. Figures were prepared using PYMOL (*The PyMOL Molecular Graphics System, Version 1.8 Schrödinger, LLC., n.d.*).

Analytical ultracentrifugation and hydrodynamic.

Sedimentation coefficients were determined at 20°C, using a Beckman Coulter XL-I centrifuge equipped with an AN60-Ti rotor equipped with Rayleigh interference detection. Samples diluted in 20 mM Tris-HCl (pH 7.5), 6 mM MgCl₂ were centrifuged for 17 h at 36 000 rpm and profiles were recorded every 5 min. Sedimentation scans were analyzed by the continuous size distribution procedure c(S) with the program Sedfit 15.01 (available at analyticalultracentrifugation.com). All c(S) distributions were calculated with a fitted frictional ratio f/f_0 and a maximum entropy regularization procedure with a confidence level of 0.95.

The theoretical sedimentation coefficients of the different atomic models were calculated using HYDROPRO (Ortega et al., 2011) and compared to the experimental sedimentation coefficients obtained from ultracentrifugation analysis.

Small-angle X-ray scattering.

For GyrBA57 apo and GyrBA57_{ΔC-loop}, protein (50μl at 7mg/ml) was eluted into buffer D5 (20 mM Tris-HCl (pH 7.5), 6 mM MgCl₂, 5% (v/v) glycerol,) plus 100 mM KCl. For GyrBA57 holo 2 mM AMPPNP and 2 mM MgCl₂ were added to the buffer and the sample. SAXS data were collected in line at beamline SWING at the synchrotron SOLEIL after elution on an increase superose 6 column (5 x 150 mm). The curves were background-subtracted using FOXTROT. Data were then processed using the HPLC-SAXS module of US-SOMO. Then, data were analyzed using the ATSAS 2.7.1 software suite. The normalized Kratky was calculated according to (Durand et al., 2010, Pérez et al., 2001) using the value determined by Guinier analysis. $P(r)$ functions were computed from the scattering curves by an indirect transform method in GNOM (Svergun, 1992), and theoretical scattering curves for model structures were calculated with CRY SOL (Svergun et al., 1995). Atomic models were refined using Dadimodo (Evrard et al., 2011, Mareuil et al., 2007, Roudenko et al., 2018) with flexibility introduced in the region corresponding to the hinge between ATPase and Toprim domains (residues 427 to 453). 20 independent calculations were carried out for each system.

BLAST searches on the region-loop and the DEEE motif.

For the C-loop, BLASTP and TBLASTN searches using a 65-amino acids peptide that includes at its center the 32-amino acids insert as a query were performed against the microbial database. The length of the peptide was chosen in order to specifically hit DNA gyrase sequences. BLAST searches for the C-loop and the ²¹¹DEEE²¹⁴ motif were performed in each bacterial phylum. In the phylum

Actinobacteria, BLAST searches were performed in each class and in each order for the class Actinobacteria.

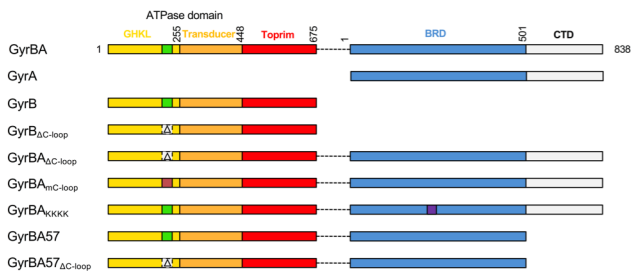
QUANTIFICATION AND STATISTICAL ANALYSIS

Each data point represents three trials, usually with the same stocks of enzymes and substrates. Error bar represent the standard error of the mean (SEM).

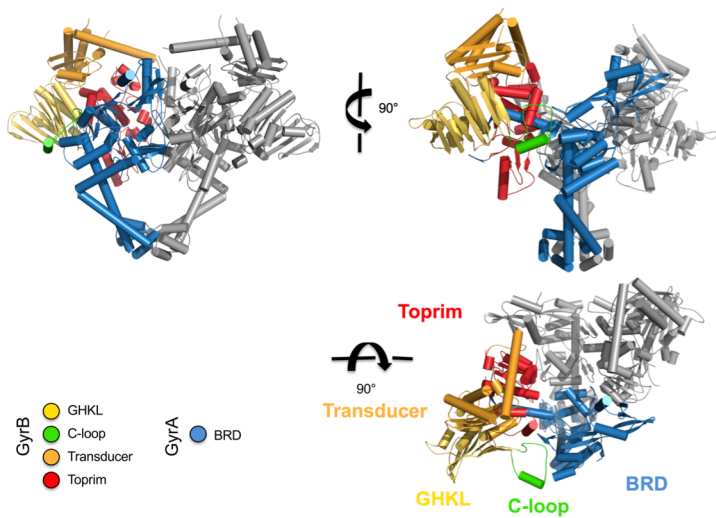
DATA AND SOFTWARE AVAILABILITY

Coordinates and structure factors have been deposited in the Protein Data Bank under accession codes 6GAV (apo) and 6GAU (holo=AMPPNP-bound).

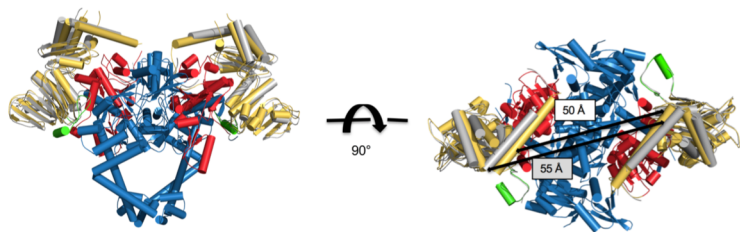
A



B



C



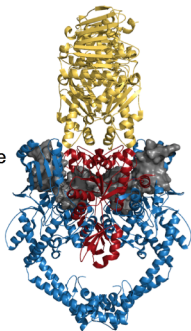
A

All gates closed

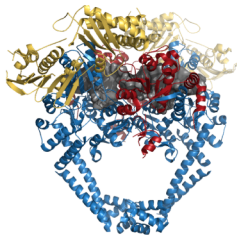
N-gate

DNA-gate

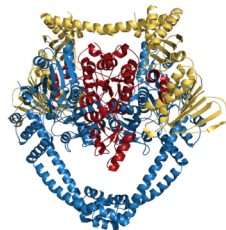
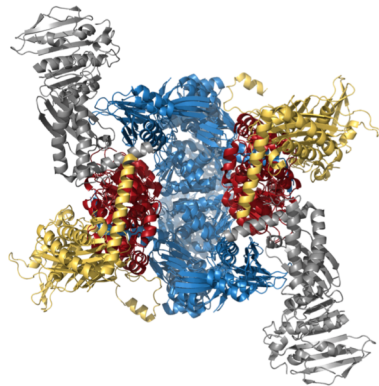
C-gate

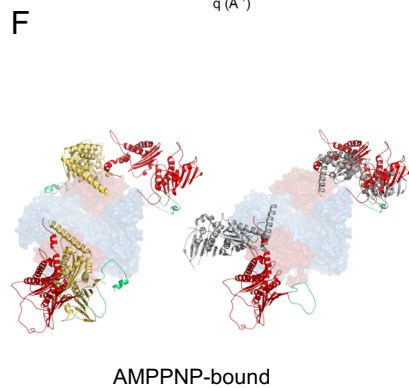
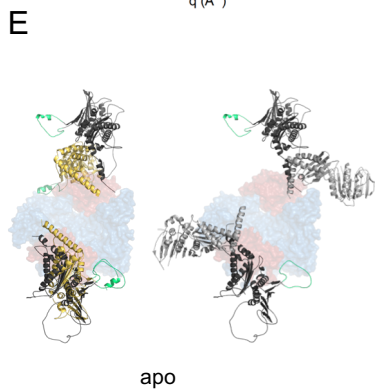
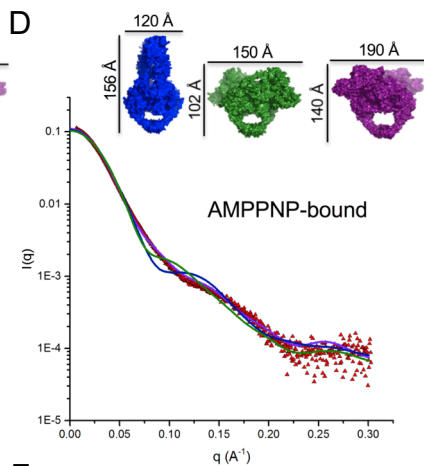
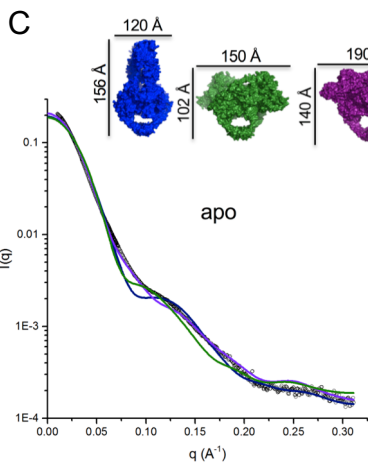
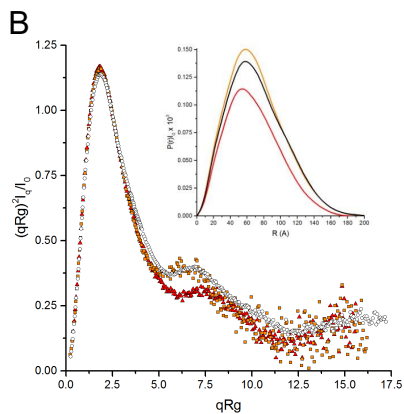
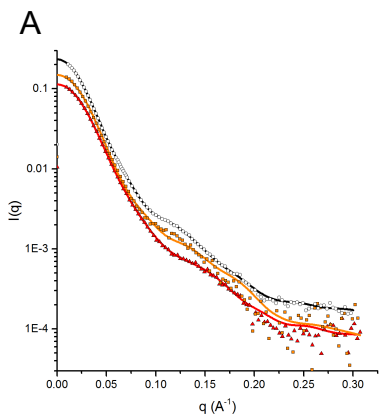


Topo II

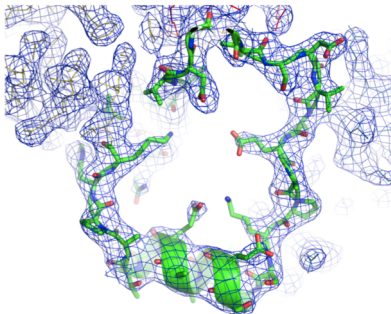
N-gate open
DNA- and C-gates closed

Topo IV

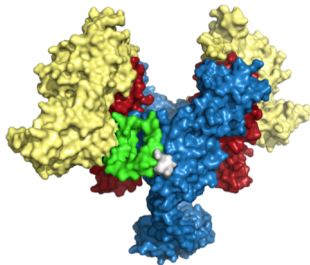
DNA gyrase
(current study)**B**



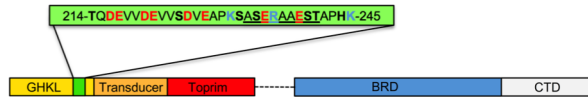
A



C

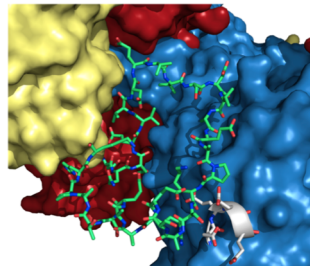


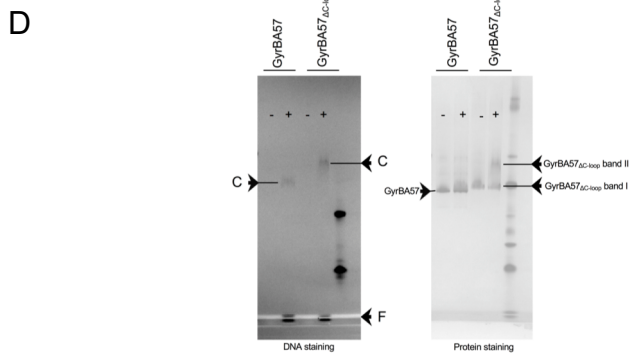
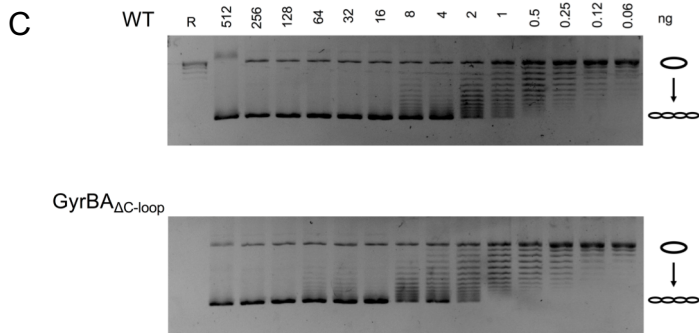
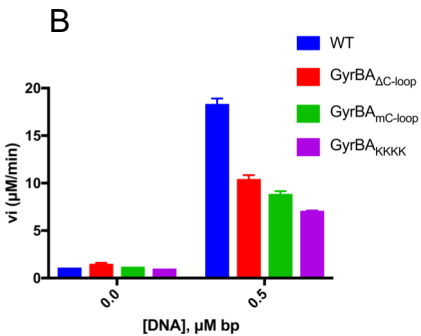
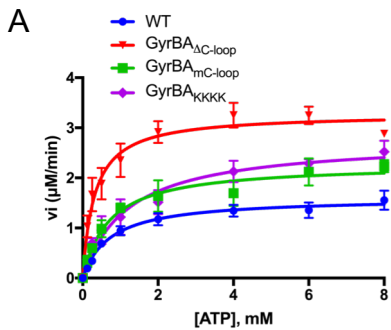
B

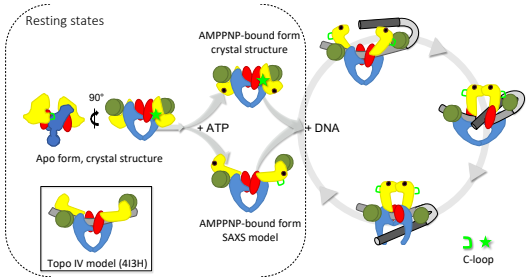


	β10		β11
GYRB_MYCTU	203 GLTINLTDERVTQDEVVDEVVS...DVAEAPKSA.....SERRAAESTAPHKVKSRTPH ₂₅₂		
GYRB_NOCBR	GLTITLTDERVSEITDDVVS...ETAEPKHA.....EADAEAPVEHKVTRRTYH		
GYRB_GORPA	GLTITLTDQRPQAVEAPGDGNGDSEPSTAEVAEV.....KSETEKAEAAKPKTRTY		
GYRB_SEGRO	GLIITLTDLREGQIDAEDGEAL...DTAEVA.....RSEQEAQAQAPVKKREYH		
GYRB_TSUPA	GLTITLTDERPVAIEVPDEDITEEAPSAHEED.....VAAALAEVAPKKRERIFH		
GYRB_CORRE	GLTINLIDERPQVEAEDELADAAE...DADAPKT.....SEEKAQEEKAKKEPKTKTFH		
GYRB_CORGL	GLTITLTDNRATDEELELEALAEQGETATELSLDEIDNETELVEETTDAPKKPKKREKKKIFH		
GYRB_ECOLI	GVSIRLRDKRDG.....KEDHFP		
PARE_STRPN	NVTLSLTDKRTD.....EAIEFH		
TOPOII_SC	DINVYLNK.....SLKIRN		

D

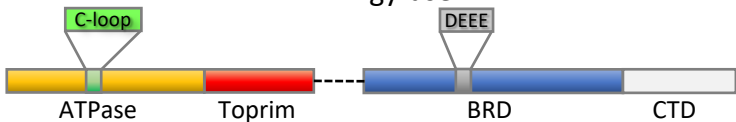






Mycobacterium tuberculosis

DNA gyrase



N-gate lies in an “extremely open” conformation stabilized by the C-loop, a *Corynebacteriales* specific GyrB insert

